29

Extremely Wetting Pattern by Photocatalytic Lithography and Its Application

Yuekun Lai[1,2], Changjian Lin[1*] and Zhong Chen[2*]
[1]*State Key Laboratory for Physical Chemistry of Solid Surfaces and College of Chemistry and Chemical Engineering, Xiamen University*
[2]*School of Materials Science and Engineering, Nanyang Technological University*
[1]*China*
[2]*Singapore*

1. Introduction

Wettability is an important property governed by not only chemical composition, but also geometrical structure as well (Ichimura et al., 2000; Lai et al., 2009a; Wang et al., 1997). Super-wetting and antiwetting interfaces, such as superhydrophilic and superhydrophobic surfaces with special liquid-solid adhesion have recently attracted worldwide attention. Superhydrophilicity and superhydrophobicity are defined based on the conventional water contact angle experiment. If the contact angle is smaller than 5°, the surface is said to be superhydrophilic. Superhydrophobic refers to surface with contact angle greater than 150°. Such two extremely cases have attracted much interest due to their importance in both theoretical research and practical application (Lafuma & Quéré, 2003; Liu et al., 2010; Gao & Jiang, 2004).

In recent years, patterned thin films have received considerable attentions due to their interesting properties for a range of applications, such as optoelectronic devices, magnetic storage media, gas sensors, and fluidic systems. Compared to the conventional thin film technology, such as physical vapor deposition (Li et al., 2006; Zhang & Kalyanaraman, 2004), chemical vapor deposition (Jeon et al., 1996; Slocik et al., 2006) and sputtering (Rusponi et al., 1999), solution-based deposition method is becoming popular for the fabrication of patterning films due to the low temperature process under ambient environment, less energy and time consumption, and easier control of the experimental parameters (Lai et al., 2010a; Liu et al., 2007; Yoshimura & Gallage, 2008). Although traditional photolithographic technique is excellent for preparing sub-micrometer or even only sub-100-nanometer pattern (Cui & Veres, 2007; Li et al., 2009), it is a complex multi-step process (wafer cleaning; barrier layer formation; photoresist coating; soft-baking; mask alignment; exposure and development; and hard-baking) and needs to remove part of the film and all the photoresist used. Direct and selective assembly of nanostructured materials from precursors paves a new avenue for the fabrication of electronic optical microdevices.

Wetting micropatterns with different physical or chemical properties, without the need for ultra-precise positioning, have frequently been acted as templates for fabricating various functional materials in a large scale. The great difference in contact angle of the two extreme cases provides a potentially powerful and economical platform to directly and precisely construct patterned nanostructures in aqueous solution. In general, wetting micropatterns

with low contact angle contrast (≤120°) on smooth substrates can be formed by photolithography (Falconnet et al., 2004; Kobayashi et al., 2011), microcontact lithography (Csucs et al., 2003; Kumar et al., 1992), colloidal patterning (Michel et al., 2002; Bhawalkar et al., 2010), electron beam lithography (Wang & Lieberman, 2003; Zhang et al., 2007), nanoimprint lithography (Jiao et al., 2005; Zhang et al., 2006), dip-pen nanolithography (Huang et al., 2010a; Lee et al., 2006; Xu & Liu, 1997), and so on. Among these methods, photocatalytic lithography employing semiconductors to photocatalytic decompose of organic monolayer is one of the most practical techniques because it able to accurately transfer an entire photomask pattern to a target substrate at a single exposure time under environmental condition (Bearinger et al., 2009; Lee & Sung, 2004; Nakata et al., 2010; Tatsuma et al., 2002; Wang et al., 2011). Moreover, it can greatly reduce the photoresist waste. The resolution of the patterning is greatly dependant on the mask alignment and light source exposure. Under optimal condition, a resolution of micrometer- or submicrometer-scale pattern of alkylsiloxane self-assembled monolayers can be achieved with UV light projection irradiation. Once patterned on the surface, organic monolayer has been applied in various ways to restrict corrosion or induce nanostructures growth. Firstly, patterned layer itself may serve as etching mask to protect the substrate to generate pattern with certain thickness/aspect ratio. Secondly, patterned organic layer may be employed as barrier to inhibit the liquid phase deposition of nanostructures to generate functional composite pattern with diverse shape and density. So far, only a few reports have been available on the fabrication and application of superhydrophilic–superhydrophobic patterning by photocatalytic lithography under ambient conditions (Lai et al., 2008a; Nishimoto et al., 2009; Zhang et al., 2007).

Upon UV irradiation, the electron-hole pairs in semiconductor TiO_2 can be generated and migrated to its surface, where the hole reacts with OH- or adsorbed water to produce highly reactive hydroxyl radicals (Zhao et al., 1998). These hydroxyl radicals can further oxidize and decompose most organic compounds. Recently, we found that the pollutant solution can be rapidly decomposed on a nanotube array TiO_2 film with UV irradiation (Lai et al., 2006, 2010b; Zhuang et al., 2007). Considering its effectiveness for the photocatalytic decomposition of organic compounds, the photocatalysis of such TiO_2 nanotube film can be a promising way to decompose the low energy hydrophobic fluoroalkyl chains. So it is possible to achieve a conversion from superhydrophobicity to superhydrophilicity due to the amplification effect of the rough aligned nanotube structure. By using a patterned photomask to control the site-selective decomposition by UV light, that is photocatalytic lithography, superhydrophilic cells can be accurately transferred to a target substrate at a single exposure time under environmental condition. Therefore, these two types of extreme wettability coexist on the surface directly to make up of superhydrophilic-superhydrophobic pattern.

In this chapter, we firstly discuss the wettability on TiO_2 nanostructure film by electrochemical anodization. Secondly, we demonstrate using a novel synthetic process to prepare wetting pattern with a high contrast (superhydrophilic–superhydrophobic) on TiO_2 nanotube structured film by a combination of SAM technique and photocatalytic lithography. The resultant micropattern has been characterized with scanning electron microscopy, optical microscopy, electron probe microanalyzer and X-ray photoelectron spectroscopy. Finally, we focus on the technological details and potential future application of wetting template to induce and direct the assembly of functional nanostructure to form uniform micropatterns. For example, the patterning, biomedical and sensing application of

the wetting template and functional composite nanostructure pattern (TiO_2, ZnO, OCP and CdS) (Lai et al., 2009b, 2010a-d).

2. Wettability on TiO_2 nanostructures by electrochemical anodization

Wettability of solid surfaces is a very important property of solid surface. Surfaces with extreme wetting properties, e.g. superhydrophilic and superhydrophobic, can be prepared by introducing certain rough structures on the originally "common" hydrophilic and hydrophobic surfaces. Various ways of preparing TiO_2 semiconductor films on the different solid substrates have been developed, including sol-gel technique (Shen et al., 2005), sputtering (Takeda et al., 2001), chemical vapor deposition (Rausch & Burte, 1993), liquid phase deposition (Katagiri et al., 2007), hydrothermal (Yun et al., 2008), and electrochemical anodizing. Among them, the electrochemical anodizing is verified to be a convenient technique for fabricating nanostructured TiO_2 films on titanium substrates (Lai et al., 2004, 2008b, 2009c; Gong et al., 2003). Moreover, the conductive titanium support substrate can be an advantage for fabricating functional material composites through electrochemical depositions to further improve their photoelectrochemical activities.

Figure 1a shows a typical FESEM image of the titanium substrate before electrochemical anodization. The surface of the substrate was relatively smooth, with features of parallel polished ridges and grooves at the micron scale (Lai et al., 2010a). Figure 1b shows the top view SEM image of the typical TiO_2 nanotube array film by anodizing under 20 V for 20 min. After anodization, shallow cavities as large as several micrometers in diameter were present on the surface of the sample. This is probably due to the anisotropic oxidation of the underlying Ti grains (Crawford & Chawla, 2009; Yasuda et al., 2007). From the high magnification image (Fig. 1c), it can be seen that vertically aligned TiO_2 nanotubes with inner diameter of approximately 80 nm covered the entire surface including the shallow polygonal micropits. The side view image shows that the self-assembled layers of the TiO_2 nanotubes were open at the top and closed at the bottom with thickness about 350 nm (inset of Fig. 1c). Water droplet can quickly spread and wet the as-grown vertically aligned TiO_2 nanostructure film due to capillary effect caused by the rough porous structure, indicating such TiO_2 structure film by electrochemical anodizing is superhydrophilic. A more hydrophobic behaviour, on the other hand, was obtained after coating the TiO_2 film with fluoroalkyl silane. The inset of Fig. 1b shows the intrinsic contact angle (CA) on the as-prepared vertically aligned TiO_2 nanotube surface and its corresponding 1*H*,1*H*,2*H*,2*H*-perfluorooctyltriethoxysilane (PTES, Degussa Co., Ltd.) modified surface is nearly 0^o (superhydrophilic) and 156^o (superhydrophobic), respectively. However, the CA for the "flat" TiO_2 surface and its corresponding PTES modified sample is about 46^o (hydrophilic) and 115^o (hydrophobic), respectively. From these results, we know the top surface of the vertically aligned nanotubes has an amplification effect to make hydrophilic and hydrophobic surfaces become superhydrophilic and superhydrophobic, respectively. After UV irradiation for 30 min, the water CA on the TiO_2 nanotube film and "flat" TiO_2 film decreased to 0^o and 26^o, as a consequence of the photocatalytic activity of TiO_2 films (Balaur et al., 2005; Lai et al., 2010a). Moreover, the sample showed hydrophobic character once again when it was treated with PTES. Therefore the surface can be reversibly switched between superhydrophobic and superhydrophilic by alternating SAM and UV photocatalysis on the rough TiO_2 nanotube arrays (shown in Fig. 1d). Compared with the large wettability contrast on this type of rough surface (larger than 150^o), the wettability of a "flat" TiO_2 film can only be reversibly changed within the small range between 26^o and 115^o.

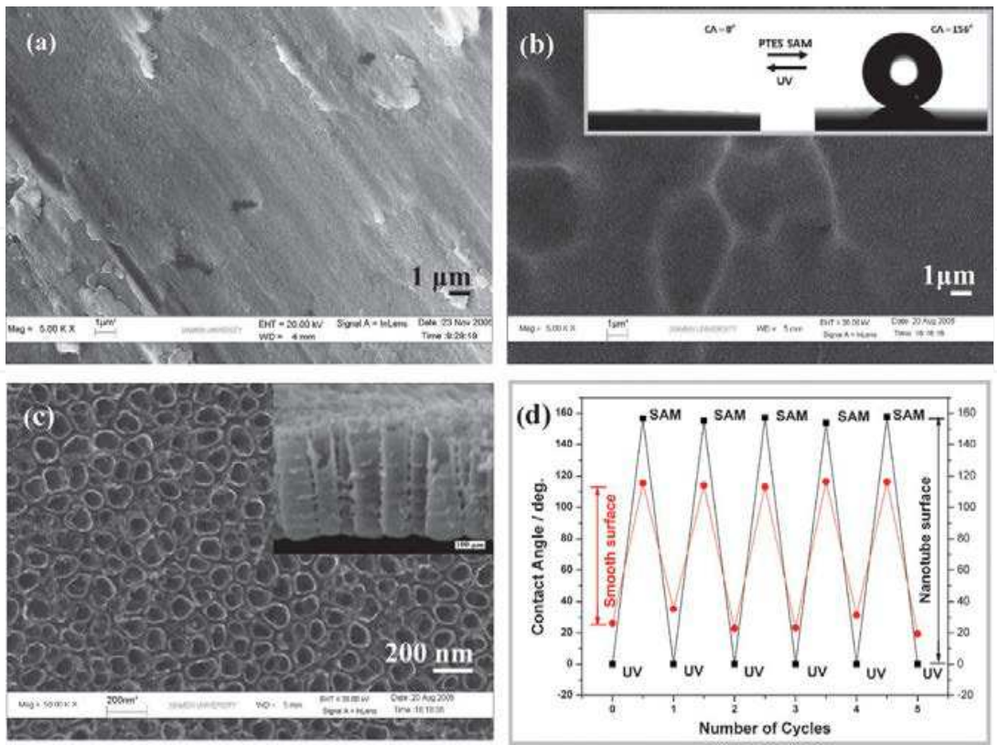

Fig. 1. SEM images of the mechanically polished and cleaned titanium substrate (a), low magnification of a nanotube structured TiO_2 film (b), and a higher magnification of the TiO_2 nanotube array film (c). Reversible surface wettability on a ''flat'' TiO_2 film and rough nanotube TiO_2 film by alternating SAM and UV photocatalysis (d). The inset of (b) shows the shape of a water drop on the PTES-modified and UV-irradiated TiO_2 nanotube array film. The inset of (c) shows the side view of a TiO_2 nanotube array film.

Recently, we designed three types of superhydrophobic nanostructure models consisting of a nanopore array (NPA), a nanotube array (NTA), and a nanovesuvianite structure (NVS) apply a facile electrochemical process (Figure 2) (Lai et al., 2009a). Based on basic principles of roughness-enhanced hydrophobicity and capillary-induced adhesion, these different porous structures were expected to create interfaces with decreasing adhesive forces. The surface adhesive forces could be effectively tuned by solid–liquid contact ways at the nanoscale and air-pocket ratio in open and sealed systems. The magnitude of the adhesive force of a droplet for a superhydrophobic surface descends in the order "area-contact" > "line-contact" > "point-contact". A continuous three-phase (solid–air–liquid) contact line (TCL) generates serious CA hysteresis and surface adhesion, while a discrete TCL is energetically advantageous to drive a droplet off a superhydrophobic surface, showing lower surface adhesion. Therefore, the water droplet behavior on these superhydrophobic surfaces could be greatly changed from pinning to sliding by adjusting the solid-liquid contact way.

Capillary adhesive force plays a dominant role in imparting adhesive behavior on NPA and NTA nanostructures will sealed cells, while the open NVS nanostructure, which had extremely low adhesion capacity for water, acted solely by van der Waals attraction between water and PTES molecules. A possible explanation is as follows. As the droplet gradually retracted from the sample surface, the meniscus on each nanotube nozzle would be changed

from concave to convex (Figure 3a). This could result in an increased volume of air sealed in each nanotube by the liquid/air interface. According to Boyle's law (West, 1999), there is an inverse relationship between the volume (V) and pressure (P) for an ideal gas under the conditions of constant temperature and quality. Therefore, this expansion of air would result in the formation of a negative pressure (ΔP). In this case, the volume of air sealed in the nanotubes was varied by their depths, so longer tubes would be expected to have lower air-expansion ratios (ΔV/V), thus lesser negative pressures. For a fixed nanotube diameter, a longer nanotube would therefore require a smaller pulling-off force, and the total surface adhesive force would be smaller.

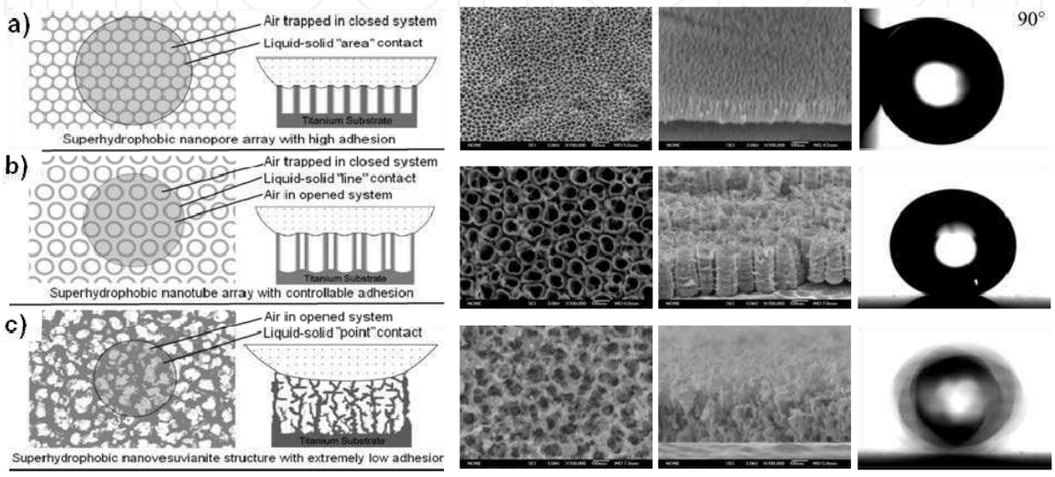

Fig. 2. Schematic models, SEM images and corresponding water behavior on three types of superhydrophobic porous-nanostructure with water adhesive forces ranging from high to low. (a) Superhydrophobic NPA with high adhesion. (b) Superhydrophobic NTA with controllable adhesion. (c) Superhydrophobic NVS with extremely low adhesion.

Figure 3b shows the curves of the water CAs and adhesive forces with respect to the diameter of individual nanotube. When the nanotube diameter decreases, the force drastically increased, while the CA slightly decreased. When the diameter was tuned from 78 nm down to 38 nm, the surface adhesive force of the superhydrophobic NTA film increased 2.06 times, while the decline in magnitude of the water CA was not more than 2%, showing that the negative pressure caused by the volume change of air sealed in the nanotubes could effectively tune the surface adhesive force. The NTA structures in this study had variable length, with values of (0.35 ± 0.04) μm, (0.76 ± 0.05) μm, (1.18 ± 0.07) μm, while their diameter (~80 nm) was fixed. Figure 3c shows the curves for water CAs and adhesive forces obtained with PTES-modified NTA-nanostructure surfaces differing in nanotube length. With lengths extending from 0.35 μm to 0.76 μm and 1.18 μm, the CA change was very small, not more than 2%, which could be due to the minor variation in nanotube diameter. However, the adhesive force linearly decreased from 21.5 μN down to 16.7 μN and 12.2 μN for the above increases in length, respectively. It was evident that the water adhesive force of the superhydrophobic NTA-nanostructure surfaces could be tuned by varying the diameters and also lengths of the nanotubes. These findings are valuable to deepen insight into the roles of nanostructures in tailoring surface water-repellent and adhesive properties for exploring new applications.

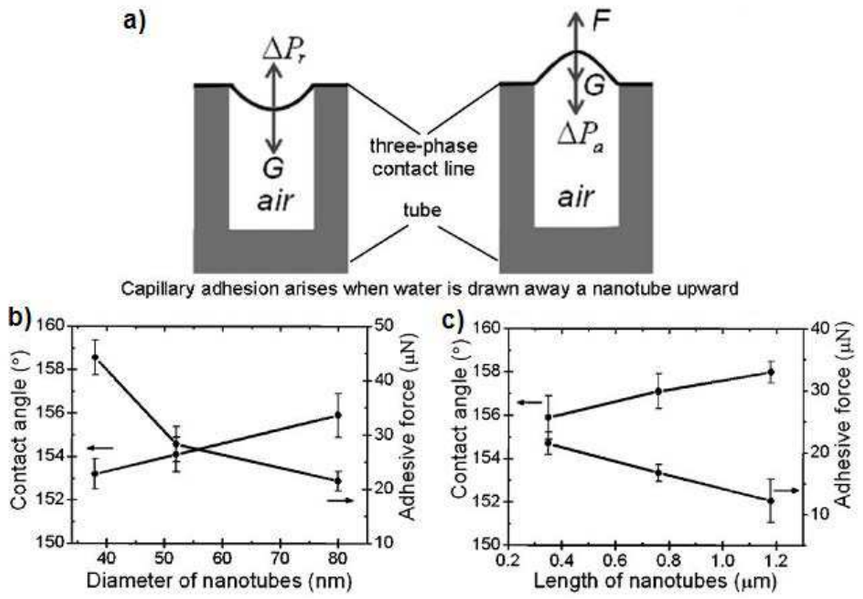

Fig. 3. (a) Capillary adhesion arises when a water droplet sitting on the tube nozzle is gradually drawn upwards because the convex air/liquid interface produces an inward pressure ΔP. (b,c) The curves of water contact angles and adhesive force on the superhydrophobic NTA nanostructures with respect to the diameter and length of nanotubes.

3. Wetting pattern by photocatalytic lithography

A novel approach for constructing superhydrophilic-superhydrophobic micropattern on the nanotube structured TiO_2 films has developed by using photocatalytic lithography (Figure 4a) (Lai et al., 2008a). At the first step, the as-prepared amorphous TiO_2 nanotubes by electrochemical anodizing of titanium sheets were calcinated at 450°C to form anatase phase, then treated with a methanolic solution of hydrolyzed 1 wt% PTES for 1 h and subsequently heated at 140°C for 1 h, and at the second step, the superhydrophobic film is selectively exposed to UV light through a copper grid (photomask) to photocatalytically cleave the fluoroalkyl chain. It is noteworthy, from the characterization of chemical composition before and after UV irradiation by X-ray photoelectron spectroscopy, that the intensities of the F1*s* and F*KLL* are decreased greatly and those of the Ti2*p* and O1*s* are increased after exposing the PTES modified surface to UV light for 20 min (Fig. 4b). From the inset high-resolution spectra (Fig. 4c), the peaks of $-CF_2$ (at 291.8 eV) and $-CF_3$ (at 294.1 eV) are obviously vanished after UV light irradiation, while the strength of silicon peaks in the XPS spectra remains unchanged but shifts from 102.8 to 103.3 eV, suggesting that Si-O-Si networks have already formed due to UV irradiation. According to these results, we believe that the hydrophobic fluoroalkyl chains have been completely decomposed and removed by the photocatalytic reactions at TiO_2 nanotube films. Similarly, a serial of fluoroalkyl silane monolayer pattern (e.g. heptadecafluorodecyltrimethoxysilane, octadecyltriethoxysilane, and methyltriethoxysilane) can be successfully fabricated in our case. Although various monolayer patterns can be prepared with a resolution about micro-scale or submicro-scale under optimal condition, we will focus on the application of the PTES micro-pattern with a general TEM copper grid as a photomask by photocatalytic lighography.

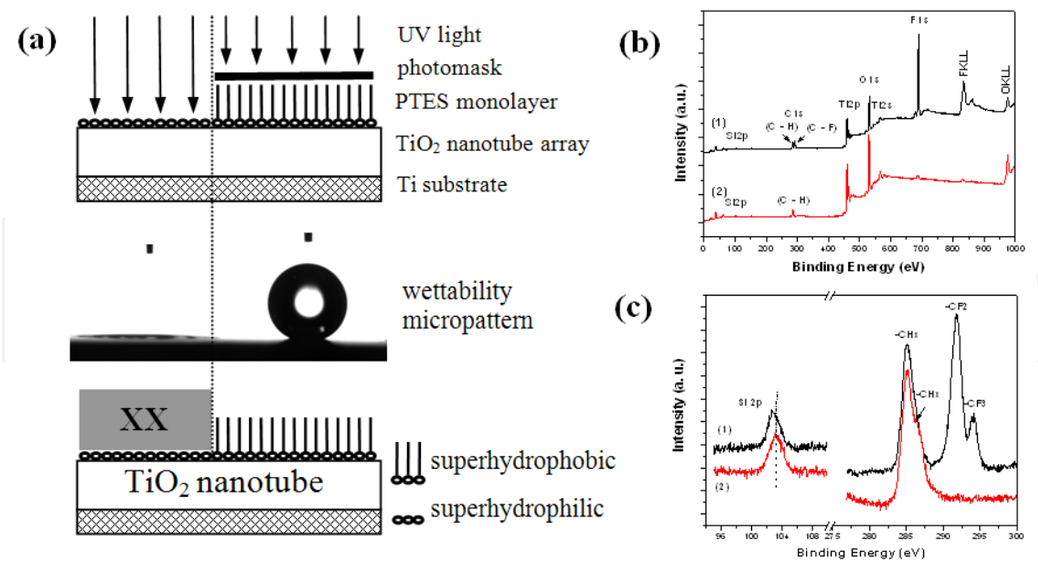

Fig. 4. Schematic outline of the procedures to fabricate nanostructured patterning film by electrochemical deposition based on superhydrophilic-superhydrophobic micropattern (a). Survey-scan X-ray photoelectron spectra of the PTES modified nanotube TiO_2 films before (1) and after (2) 20 min UV irradiation (b). The high-resolution spectra of Si2*p* and C1*s* regions (c).

Figure 5 shows the optical micrograph of the as-obtained superhydrophilic–superhydrophobic pattern by focusing on the droplet within the superhydrophilic regions. A uniform pattern is formed due to the site-selective wetting by water droplets within the superhydrophilic regions (Fig. 5a). A light dot array (inset of Fig. 5a) is seen when focusing on the top of the droplets, indicating that the confined droplet has a hemispherical dome. To further verify the resulting micropatterns with an extreme wettability contrast, fluorescein sodium was used as a probe to label the surface of the films. Figure 5b shows the fluorescent micrograph of the resultant superhydrophilic–superhydrophobic micropatterns on the TiO_2 nanotube array films. As shown, geometrically identical square superhydrophilic regions and dark superhydrophobic regions transferred well from the photomask to form a well-defined pattern. The UV-irradiated regions become superhydrophilic owing to the photocatalytic cleavage of the PTES molecule and the enhanced roughness of the nanotube structure, while the non-irradiated parts remain superhydrophobic without any change. Because the difference in the water CA between the irradiated and non-irradiated regions is larger than 150°, the liquid containing the fluorescent probe selectively appears only on the uniform superhydrophilic grids and not on the neighboring superhydrophobic regions. Therefore, a clear, well-defined fluorescent pattern in line with the dimensions of the Cu grid can be obtained. These results indicate that the micropatterned template composed of superhydrophilic and superhydrophobic regions was fabricated successfully.

The UV irradiation times had a great effect on the quality of the resulting pattern. For example, it cannot exhibit a sufficient wettability contrast between the irradiated and non-irradiated regions to form a well-defined pattern within 5 min. This is attributed to the hydrophobic fluoroalkyl chain in the PTES molecule that was not efficiently cleaved under a short-time UV irradiation. However, with a long-time UV irradiation (i.e., 60 min), the

adjacent PTES molecule covered by the Cu grid can be remotely oxidized by a TiO_2 nanotube photocatalyst or the diffusion, scattering, and diffraction of the incident light (Haick & Paz, 2001; Kubo et al., 2004). Therefore, to obtain a higher pattern resolution, the optimized UV irradiated time in our case was controlled in the range of 10-30 min.

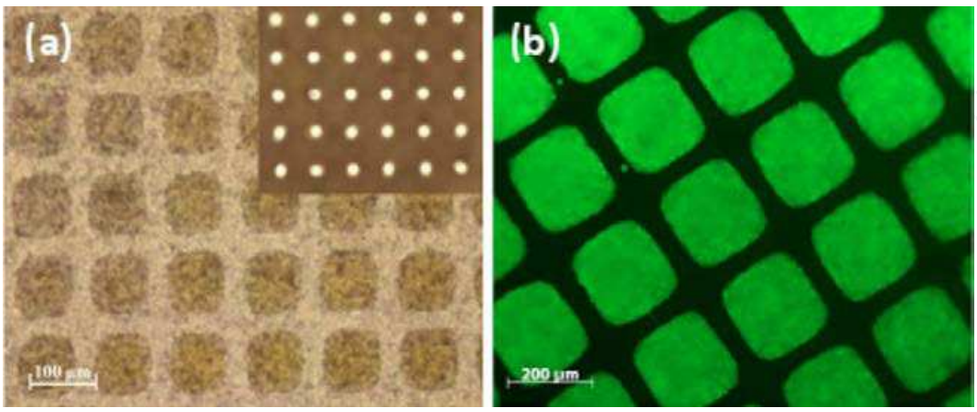

Fig. 5. (a) Optical micrograph of the as-obtained superhydrophilic-superhydrophobic pattern by focusing on the water droplet within the superhydrophilic regions. (b) Fluorescence microscopy image of the fluorescein probes on the as-prepared superhydrophilic-superhydrophobic micropattern.

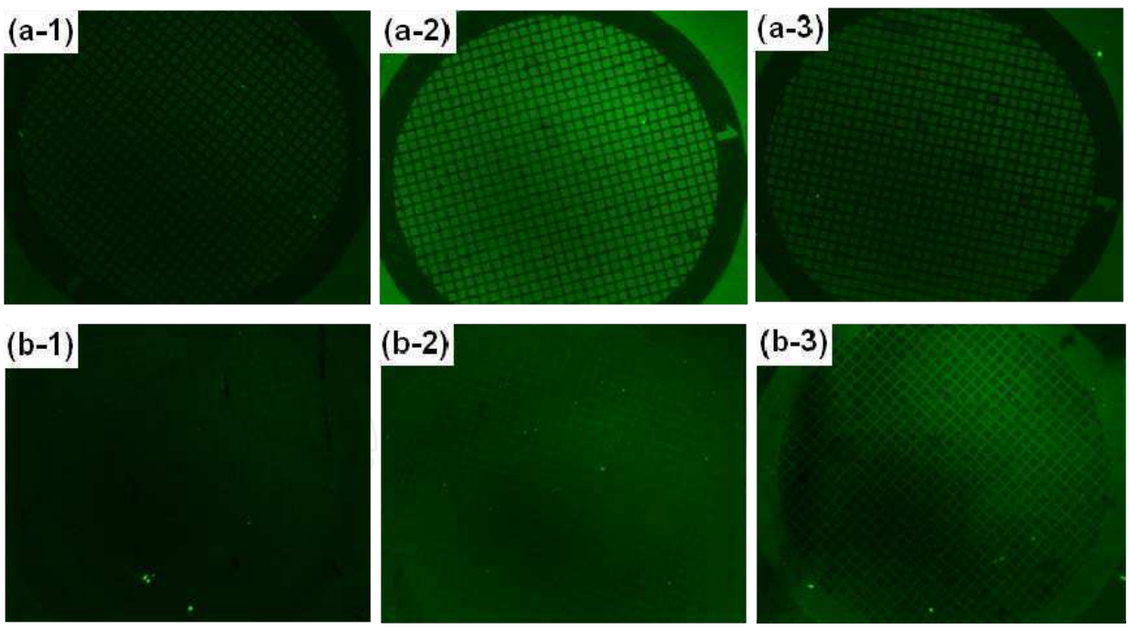

Fig. 6. Fluorescence microscope images generated by blue light excitation on the different micropatterned templates with the adsorption of FITC-BSA, (a-1, a-2, a-3) the PTES template with a pH value of 7.5, 4.5 and 2.5, respectively; (b-1, b-2, b-3) the PTES-APTS template with a pH value of 7.5, 4.5 and 2.5, respectively.

Based on the molecular self-assembly and photocatalytic lithography techniques, micropatterned templates of PTES or PTES-APTS(3-aminopropyltriethoxysilanes) with

different wettabilities were fabricated on the titania film. The adsorption behavior of bovine serum albumin (BSA) on the above two templates was investigated using fluorescent labeling (FITC) in buffer solution with different pH values. The results showed that, for the PTES template with great wettability differences, BSA would preferentially adsorb on the superhydrophilic regions. For the APTS-PTES template with smaller differences in wettability, competitive adsorption phenomenon on the super-hydrophobic regions was found due to the hydrophobic interaction force between the albumin and the surface. As the pH value decreased to 2.5, the phenomenon of competitive adsorption was prominent with the albumin adsorbed in the super-hydrophobic areas. The adsorption feature of the albumin may be closely related to the wettability and surface energy of the materials. This technique has promising applications in bio-compatible coatings where drugs could be encapsulated in specific areas of the coating using simple microfabrication methods.

4. Application of wetting pattern

Uniform self-assembly of functional inorganic nanomaterials is a fundamental challenge. Nature adopts a superior approach in biomineralization, where "matrix" macromolecules induce nucleation of inorganic crystals at specific locations with controlled size and morphology, and sometimes even with defined growth orientation. We apply the biomimetic principles derived from liquid phase processes to the assembly of nanoscale functional materials into microscale systems. We carefully control surface wettability to promote etching or heterogeneous nucleation at designated superhydrophilic regions while completely suppress these processes elsewhere (superhydrophobic regions), therefore enable the controlled top-down or bottom-up assembly of inorganic nanomaterials directly from solution. Following this principle, arrays of crystalline TiO_2 nanotube, ZnO nanorods, CdS semiconductor materials and octacalcium phosphate (OCP) biomaterials were nucleated and assembled directly from solution onto Ti substrates at the desired precise locations and then fabricated into arrays of photodetector or matrix devices for large-area microelectronic applications. This strategy of micropatterned nanocomposites will be helpful to develop various micropatterned functional nanostructured materials.

4.1 Template for preparing functional pattern

Figure 7 shows an optical microscopy image of the TiO_2 nanotube micropattern produced using a grid micropattern with different wet etching times (Lai et al., 2009b). A patterning with a clear outline was formed in a short time for 30 s (Fig. 7a). With an increase in the wet etching time (Fig. 7b and c), identical micropatterns with higher aspect ratios can be fabricated. When the etching was prolonged to 240 s (Fig. 7d), the size of the grids increased slightly, indicating that the PTES-SAM layer at the edge of the superhydrophobic lines is more easily etched as compared to the inner superhydrophobic area. This is due to the loose and disordered SAMs resulting from the scattered UV light photocatalytic degradation and the transfer of the active hydroxyl radicals at the edge of the grids. Moreover, the isotropic etching of the Ti substrate underneath the boundary leads to the collapse of the upper nanotube array structures. Therefore, the pattern can be obtained with a clear boundary in a short time after the wet etching in the aqueous solution, and the depth of the etching can be controlled simply by adjusting the etching time.

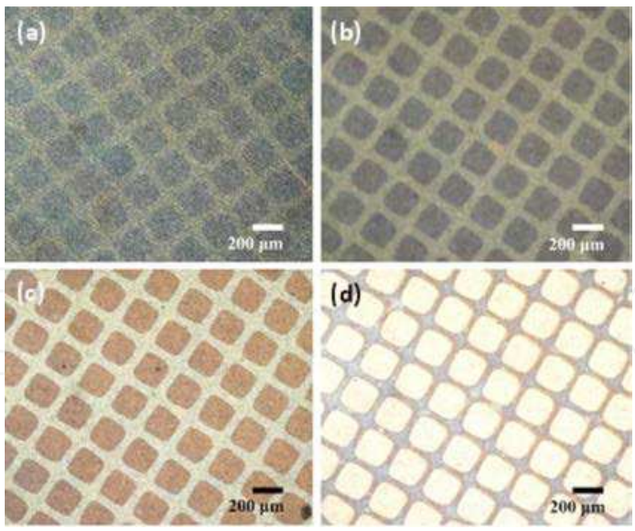

Fig. 7. Optical micrograph images of the time-resolved evolution process of the resulting vertical aligned TiO_2 nanotube micropattern on a superhydrophilic-superhydrophobic template by wet chemical etching in 0.1 wt% HF solution: (a) 30, (b) 60, (c) 120, and (d) 240 s.

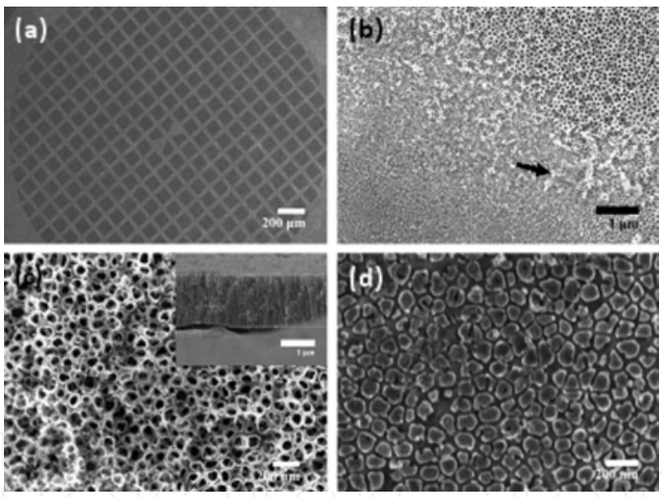

Fig. 8. (a) The SEM micrograph of the ordered vertical aligned TiO_2 nanotube array pattern by vapor-condense etching for 10 min. Magnified images of the corresponding (b) superhydrophilic-superhydrophobic boundary, (c) superhydrophobic area, and (d) superhydrophilic area. The inset figure shows the corresponding cross-sectional image.

The micropattern with a higher aspect-ratio can also be fabricated by a developed vapor etching technique. As water evaporated, the vapor containing HF dewetted the superhydrophobic lines while condensing on the superhydrophilic grids to etch the vertical aligned TiO_2 nanotube layer. Figure 8a and b shows the as-prepared TiO_2 micropattern with a clear boundary by water vapor etching for 10 min. This resulted from the selective condensing of the vapor from the water solution containing 5 wt% HF in the superhydrophilic regions. Some collapsed residue (indicated by the black arrow) covers the boundary due to the rapid etching of the bottom nanotubes and the resultant bubbles;

however, they can be easily removed by sonication. The vertical aligned TiO_2 nanotube film with a length of about 1.53 μm shows no obvious change within the superhydrophobic regions (Fig. 8c), while the TiO_2 nanotubes in the superhydrophilic regions are etched completely for 20 min (Fig. 8d), that is to say, a TiO_2 micropattern with a high aspect ratio of ~20 can be obtained. This technique is particularly attractive in generating large-area functional nanostructure patterns in a high throughput fashion with a high aspect-ratio.

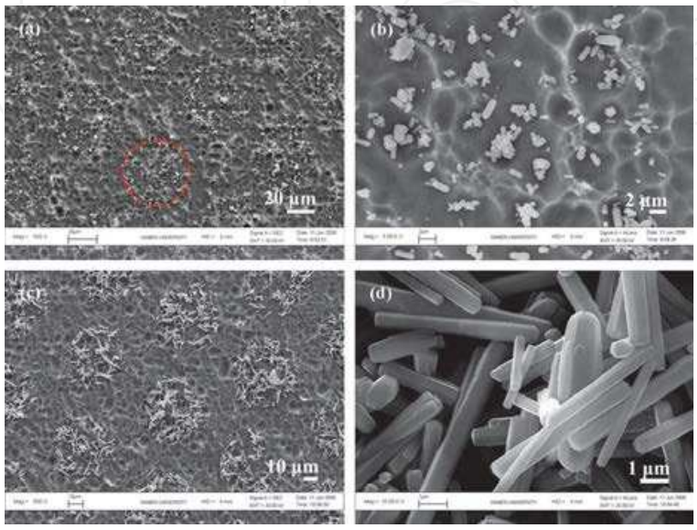

Fig. 9. SEM images of the patterned ZnO nanostructured micropatterns by liquid phase deposition at 90°C for different times: (a, b) 30 min; (c, d) 90 min.

Figure 9 shows representative top-view FESEM images of the ZnO/TiO_2 micropatterns by liquid-phase deposition after different times. After growth for 30 min (Fig. 9a,b), the nucleation and growth of ZnO crystals with various morphologies and sizes (nanoparticles and nanorods) are sparsely dispersed within the predefined superhydrophilic regions. In the superhydrophobic regions, the nanotube structure is retained with its original morphology due to the indirect contact with the solution and the effective protection by the PTES monolayer. Upon further increase in the deposition time to 90 min (Fig. 9c,d), it was observed that ZnO nanorods were the predominant structural features. The average diameter of the grown ZnO nanorods increases greatly to about 400–800 nm in diameter and 3-5 μm in length, which may be due to lower nucleation rate and higher growing space for ZnO nanorods. The superhydrophilic microdots are almost covered with randomly lying ZnO nanorods. Moreover, there are different growth orientations and some connections into adjacent nanorods. It is of interest to note that a two dimensional (2D) pattern with smaller density of randomly packed ZnO nanorods, instead of the 3D pattern consisted of well-aligned vertical nanorods, which were confined and grown within the superhydrophilic regions.

For practical application of thin film devices, the position and orientation-control of ZnO nanorods are very important because they directly relate to their physical and chemical performances (Koumoto et al., 2008; Masuda et al., 2006). In order to precisely control the spatial orientation of the ZnO nanostructures, we developed a new technique which is able to make the ZnO nanorods grow along the vertically aligned titania nanotubes rather by disordered deposition on the titania nanotube array surface. In this technique, resistance discrepancy was adopted to make the entrance of the tubes more conductive than the bottom of the tubes, to induce the epitaxial growth with spatial organization of uniform

ZnO nanorods along the direction of the nanotubes. The quasi-perpendicular ZnO nanorods nucleate and grow uniformly and selectively throughout the superhydrophilic regions of the TiO_2 nanotube surface by electric field assisted deposition at 90°C for 3 min, while no nanorods are observed in the superhydrophobic regions (Fig. 10a,b) (Lai et al., 2010a). The EDS spectra also reveal that the presence of Zn, Ti and O elements on the superhydrophilic regions, while the elemental components in the superhydrophobic areas are only Ti and O. The inset of Fig. 10b shows the hexagonal end facet of a vertically aligned ZnO nanorod with a diameter about 100–150 nm growing on top of the TiO_2 nanotube array surface. Therefore, the density, size and orientation of ZnO nanorods are very sensitive to the presence of electric fields. A 3D AFM profile image (Fig. 10c) shows that the microscopic structure of the ZnO crystal deposition consisted in dense column arrays, which are induced and directed by the wettability template. The thickness of vertical ZnO nanorod film is in the range of 800–900 nm. Furthermore, the three dimensional confocal microscopy image (Fig. 10d) also shows that the growth of the ZnO nanorod pattern is identical with the superhydrophilic/superhydrophobic template.

On the basis of the versatile superhydrophilic-superhydrophobic template, we can successfully control the growth of ZnO nanostructures in the superhydrophilic regions under mild reaction conditions and in the absence of seed and noble metal catalyst. In the superhydrophobic regions, the growth is suppressed. This special template can be utilized to generate different nanostructured ZnO patterns with clearly defined edges. Hence, it is expected that this novel micropatterned technique based on the superhydrophilic-superhydrophobic template will become a powerful tool for fabricating various types of micropatterned nanomaterials and devices.

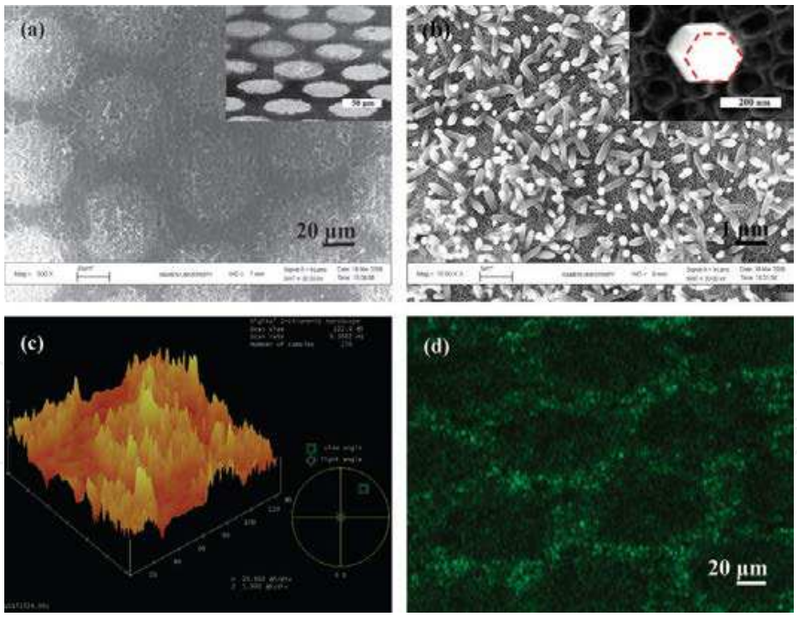

Fig. 10. (a,b) Typical SEM images of the vertically aligned ZnO nanorods selectively grown on superhydrophilic patterning regions by the developed electric field assisted deposition technique at 90°C for 3 min. The inset in (a) shows the side view SEM image of the corresponding ZnO nanorod micropattern. The inset in (b) shows the higher magnified SEM image of a ZnO nanorod with hexagonal end facet. (c) 3D AFM image of the ZnO/TiO_2 micropattern. (d) Confocal microscopy image of the perpendicular ZnO nanorod array.

4.2 Biomedical arrays

The typical SEM image of TiO_2 nanotube array surface before and after the deposition of OCP film by electrochemical technique for 5 min is shown in Fig. 11a,b. The superhydrophobic-superhydrophilic micropatterned TiO_2 was used as a micro-template to selectively deposit nano-OCP crystals on the superhydrophilic regions by an electrochemical deposition to form a special micropatterned nano-OCP. The deposition electrolyte was consisted of 0.042 mol/L $Ca(NO_3)_2$ and 0.025 mol/L $NH_4H_2PO_4$. The pH value was adjusted to approximately 4.2 with 0.05 mol/L NaOH solution. The precipitation was carried out galvanostatically at a cathodic current of 0.5 mA cm^{-2} under 67.5°C for a certain time (Wang et al., 2008). It can see that quasi-perpendicular ribbon-like crystals of several hundred nanometers in width are uniformly grown on the TiO_2 nanotube array surface. Fig. 11c shows a typical fluorescence microscope of the superhydrophilic-superhydrophobic micropattern on TiO_2 nanotube surface. As can be seen, the green dot patterns are clearly imaged through the fluorescence contrast between the UV-irradiated superhydrophilic and photomasked superhydrophobic regions. The photoirradiated dot exhibiting a uniformly stronger fluorescence against the surrounding dark background is due to the highly affinity to solution resulting in the absorption of fluorescent probes into the irradiated nanotube array films. Therefore, a clear well-defined fluorescence pattern based on the superhydrophobic-superhydrophilic pattern is obtained. Fig. 11d displays the identical patterning of OCP biomaterials deposited on the superhydrophilic-superhydrophobic patterns on TiO_2 nanotube array surface. It is obvious that the size of the white OCP dots is equal to that of the superhydrophilic area on template, indicating the deposited regions were only located within the superhydrophilic dots where photocatalytic degradation of PTES-SAMs was performed.

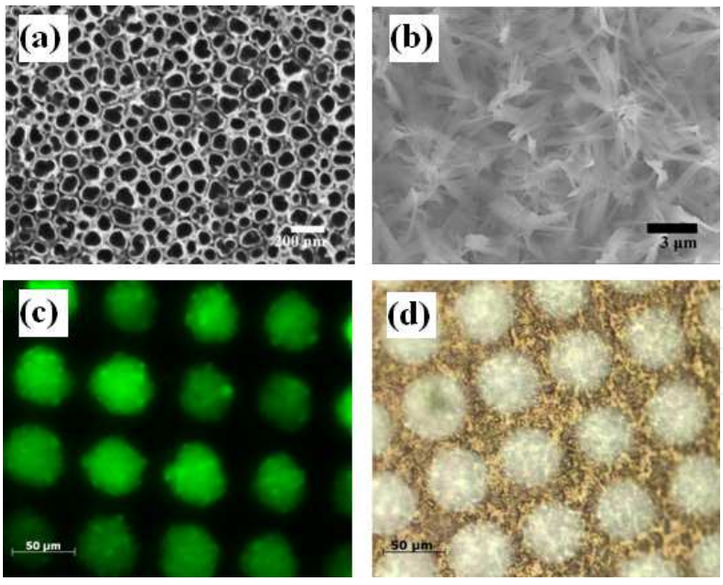

Fig. 11. SEM images of the (a) TiO_2 nanotube array film fabricated by electrochemical anodization; (b) OCP nanostructure layer on TiO_2 nanotube array film by electrochemical deposition for 5 min. Optical fluorescence pattern of the superhydrophilic-superhydrophobic template (c) and patterned OCP thin films selectively deposited in pre-defined superhydrophilic regions by electrochemical deposition for 5 min (d).

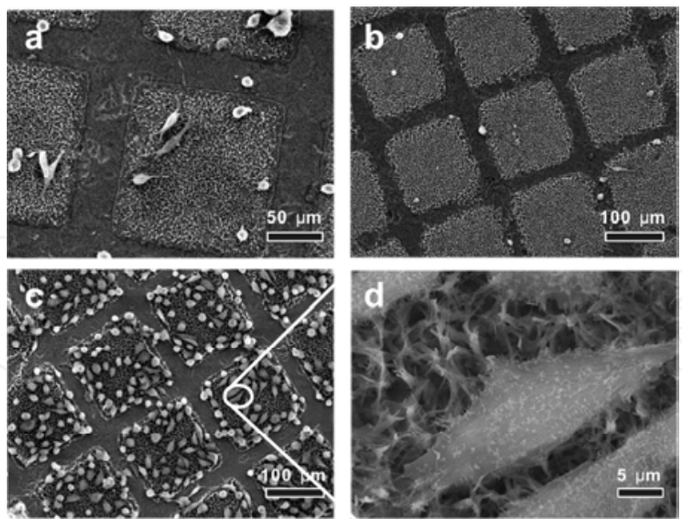

Fig. 12. SEM micrographs of MG-63 cells cultured on the patterned OCP coatings with different deposition time for 6 h, (a) 1 min; (b) 3 min; (c) 5 min; (d) higher magnification.

The *in-vitro* MG-63 cell tests were used to study the biological performance of the as-obtained OCP micropatterns (Huang et al., 2010b). The results showed that MG-63 cells were found preferentially attached on the superhydrophilic regions with OCP thin films, while the superhydrophobic regions with the PTES monolayers can effectively prevented the adhesion of cells on the surface, indicating that the cells had the selective adhesion action on the tiny units of OCP films. Moreover, the cells adhered on the OCP film deposited for a longer period (5 min) are more active to spread on the OCP nanobelt covering surface. It is promising for developing a new cell chip for high throughput evaluation of the cell behaviors.

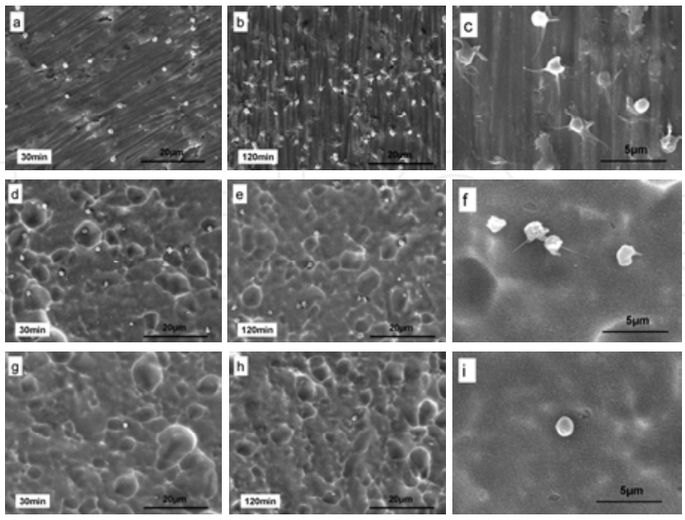

Fig. 13. SEM images of adhered platelets on various kinds of surfaces at 37◦C for different periods. (a-c) mechanically polished and cleaned Ti substrate; (d-f) superhydrophilic surface; (g-i) superhydrophobic surface; (a,d,g) 30 min; (b,e,h) 120 min; (c,f,i) magnified images of the corresponding images of (b,e,h).

The *in vitro* experimental indicated that the superhydrophobic nanotube TiO_2 layers exhibit a remarkable resistance to platelets attachment (Fig. 13) (Yang et al., 2010). It is indicated that the superhydrophobic nanotube TiO_2 layers exhibit a remarkable resistance to platelets attachment. As shown in Fig. 13a,d,g, abundant platelets adhere to both the plain Ti surface and the superhydrophilic TiO_2 nanotube layers after 30 min incubation. Comparatively, after 120 min incubation, a large number of platelets adhered and spread out on both the plain Ti surface (77 ± 7.4 per 5000 μm², Fig. 13b,c) and the superhydrophilic surface which was obtained by exposing the TiO_2 nanotubes under a UV irradiation (22 ± 1.5 per 5000 μm², Fig. 13e,f), only very few of platelets (1 ± 0.8 per 5000 μm²) was found to adhere on the superhydrophobic TiO_2 nanotube layers (Fig. 13h). Moreover, even though some platelets were occasionally seen attached on the superhydrophobic surface, they looked smooth without any growth of pseudopods (Fig. 13i), implying that the platelets adhered on the superhydrophobic TiO_2 nanotube surface remain inactive and hardly grow and spread out for a long period. The quantities and morphologies of adhered platelets and their corresponding interactions on the different samples are illustrated in Figure 14. Therefore, the construction of superhydrophobic surface on biomedical implants could pave a way to improve the blood compatibility of the biomedical devices and implants.

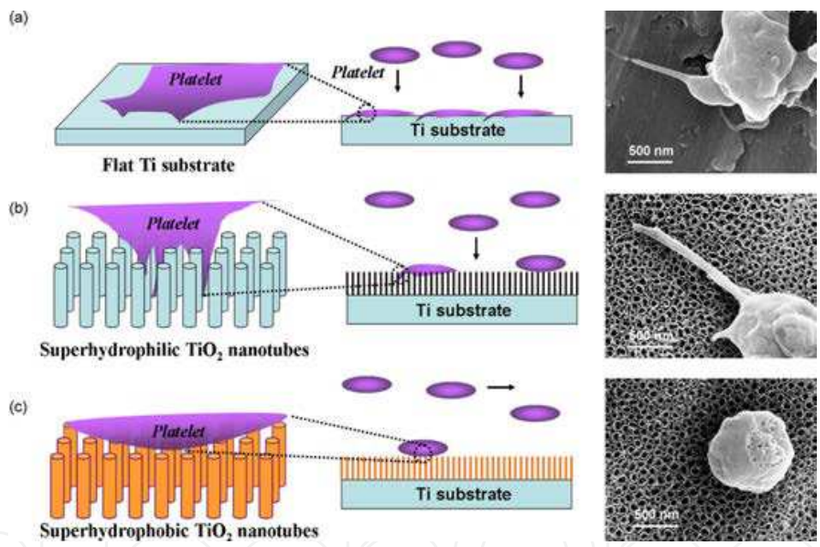

Fig. 14. Schematic illustration of the quantity and morphology of platelet and corresponding interactions on the three kinds of surfaces. (a) Plain Ti substrate; (b) Superhydrophilic TiO_2 nanotubes; and (c) Superhydrophobic TiO_2 nanotubes.

4.3 Sensing devices

Based on photocatalytic lithography, we demonstrate a facile, rapid and practical approach to fabricate Ag nanoparticle (NP) patterns on TiO_2 films by means of pulse-current electrodeposition technique (Huang et al., 2011). The size and density of as-deposited Ag NPs can be controlled by changing deposition charge density. Moreover, the resultant patterned Ag NP films exhibited particle size-as well as density-dependent UV-vis absorption and SERS enhancement effect. It was found that the patterned Ag NP films produced under the deposition charge density of 2.0 C cm^{-2} exhibited the intense UV-vis and Raman peaks. Two dimensional surface enhanced Raman scattering (SERS) mapping of

Rhodamine 6G (R6G) on the patterned Ag NP films demonstrated a high throughput localized molecular adsorption and micropatterned SERS effect.

Furthermore, the elemental distributions of the as-prepared Ag NPs arrays were also observed by electron probe microanalyzer, which are shown in Fig. 15a-c. Figure 15a shows the Ag element distribution map. As shown in the map, the green dot patterns are clearly images obtained through element concentration contrast between the UV-irradiated superhydrophilic and photomasked superhydrophobic regions. The green dots exhibiting a uniform Ag concentration against the surrounding black regions indicate that Ag NPs are uniformly deposited and confined to the superhydrophilic regions. Figure 15b,c shows the element distribution maps of Ti and O, respectively, which are also in line with the dimensions of the photomask. The blue superhydrophilic regions (dot patterns) show lower Ti and O concentrations due to the preferential deposition of Ag NPs in the superhydrophilic areas, while the yellow and red superhydrophobic regions have higher Ti and O concentration. The corresponding line-scan signal intensity profiles of Ag, O, and Ti elements across the dot pattern (red line direction). The intense Ag signals in the superhydrophilic regions as well as the Ti and O signals in the superhydrophobic regions suggest that Ag NPs are deposited only in the dot areas and that the other regions are the exposed TiO_2 nanotube films. The consistent intensity of the Ag signals indicates that Ag NPs are uniformly deposited on the superhydrophilic regions.

In addition, a two-dimensional point-by-point SERS mapping of the patterned Ag NP film whose deposited charge density is 2.0 C cm^{-2} was obtained using R6G as the probe molecule. Figure 15d,e show the optical image and the corresponding SERS mapping image of the patterned Ag NP film. The mapping area was approximately 140 × 100 μm^2 and the data acquisition time was 1 s. A signal to baseline from 594.0 to 623.4 cm^{-1} was chosen for the acquisition of the SERS mapping. The bright and dark areas respectively represent higher and lower intensity of the SERS signal. It is clear that the geometrically identical gray superhydrophilic areas (circle) with a strong SERS activity and the dark superhydrophobic areas without any SERS activity form a high-resolution SERS intensity distribution map. As can be seen from the SERS mapping results, most SERS peak area is in a very narrow intensity window as shown by the contrast in color codes. Furthermore, the SERS peak area is uniform over the superhydrophilic region with several high intensity spots represented by white color codes. On comparing the SERS mapping with the SEM detection, it is reasonable to conclude that the homogeneous SERS signal in the circle areas reflects the uniform dispersion of Ag NPs on the superhydrophilic areas. The high-resolution SERS intensity distribution and micropatterned SERS effect of the Ag NP film might make it potentially useful in high-throughput molecule detection and bio-recognition.

To gain insight into the dependence of SERS enhancement on the size and density of Ag NPs, the SERS spectra of R6G absorbed on the different patterned Ag NP films were detected, which are shown in Fig. 15f. Because of the small particle size and low density, which are not the optimum size and distribution for SERS, the signal enhancement is rather weak below the charge density of 0.5 C cm^{-2}. The enhancement behavior of the substrate, however, is obviously improved under the charge density of 1.0 C cm^{-2}. In particular, the patterned Ag NP film prepared under a charge density of 2.0 C cm^{-2} exhibits the highest intensity, which is attributed to large size and high density of Ag NPs, as shown by the SEM results. On increasing the charge density to 2.5 C cm^{-2}, the signal becomes weaker. The size-correlated enhancement may be explained by the EM mechanism (Zeng et al., 2008). The intensity of the SERS signal might also be controlled by the NPs density, which changes the

interparticle spacing as well as the hot spots among the NPs (Felidj et al., 1999; Lu et al., 2005). The average surface enhancement factor for pyridine on the Ag NP film with a charge density of 2.0 C cm^{-2} was calculated to be 1.3×10^5.

Fig. 16a shows the typical SEM micrographs of the CdS nanosphere micropatterns after 3 min deposition on the superhydrophobic-superhydrophilic template of TiO_2 nanotube films (Lai et al., 2010d). The bright rectangular areas corresponded to the deposition of CdS nanosphere crystals on the superhydrophilic regions. The boundary between the CdS pattern and the surrounding superhydrophobic regions is clearly visible at a higher magnification (inset). The dispersed CdS nanosphere crystals grew on the top of TiO_2 nanotube arrays within the rectangular superhydrophilic region (Fig. 16c). Most of the crystals were less than 90 nm in diameter due to the confinement by the inner diameter of nanotube, though a few larger spheres (~120 nm) were seen across neighboring tube openings. While on the superhydrophobic areas (Fig. 16d), there was almost no CdS crystal. The high growth selectivity was also confirmed by the EDS analysis, revealing that CdS spheres easily nucleate and grow on the hydroxyl groups (–OH) terminated regions (Fig. 16e), but not on the $–CF_3$ terminated areas (Fig. 16f). Since the difference of the water contact angle between the superhydrophilic and superhydrophobic regions is larger than 150°, electrolyte solution is preferentially presented on the uniform superhydrophilic dots. No water droplets go to the neighboring superhydrophobic regions. Although a few CdS particles resulted from homogeneous precipitation attached onto superhydrophobic surface due to van der Waals interactions and gravity, they can be easily removed by ultrasonication. Therefore, a clear and well-defined CdS pattern in line with the dimensions of the superhydrophobic–superhydrophilic template has been obtained.

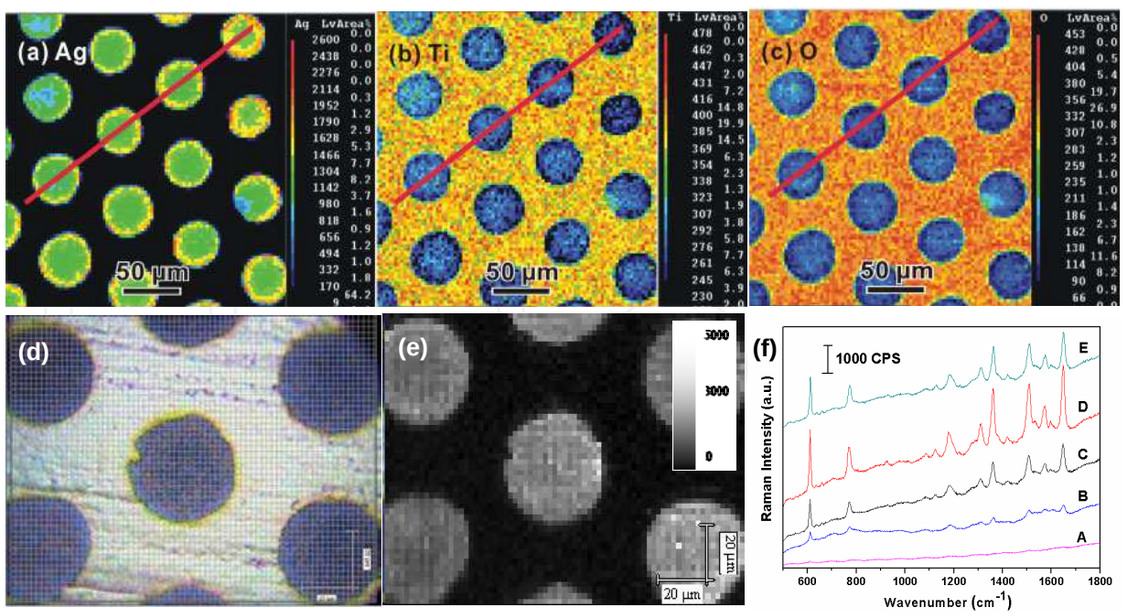

Fig. 15. Typical element distribution maps of Ag (a),Ti (b), O (c), and optical microscopy(d) and the corresponding R6G SERS mapping (e) of the patterned Ag NP films with an area of 140 × 100 μm^2 using the peak area at 614 cm^{-1} as the reference. (f) Raman spectra of the patterned Ag NP films from different charge density: curve A, bare subsrate; curve B, 0.5 C/cm^2; C, 1.0 C/cm^2; D, 2.0 C/cm^2; and E, 2.5 C/cm^2.

Fig. 16b shows the photocurrent spectra of the couple CdS/TiO_2 nanotube array electrode prepared under different electrodeposition times. It is apparent that the pure TiO_2 nanotube array samples have a photo-response wavelength lower than 400 nm due to its band-gap of 3.2 eV (curve a). The decoration of CdS nanospheres with a smaller energy band-gap (2.4 eV) can significantly extend the photo-response range from 380 nm to about 500 nm.Moreover, the CdS modified TiO_2 nanotube array electrodes can also greatly increase the photocurrent response under UV light, especially for the samples obtained under 2 min electrodeposition (curve b), which thus would be the optimal deposition time. This is attributed to the uniform dispersed CdS nanospheres with suitable size decorated onto the TiO_2 nanotubes. This allows for more efficient electron transfer and lower electron-hole recombination rate which leads to enhanced light harvesting at the directly grown CdS/TiO_2 heterojunctions. With the increase of time (curve c and d), more CdS particles with bigger size started to randomly distribute on top of TiO_2 nanotube arrays. Such composite nanostructures would weaken the light absorption of the uniform CdS/TiO_2 heterojunction underlayer, which has resulted in a lower photocurrent in both UV and visible light region.

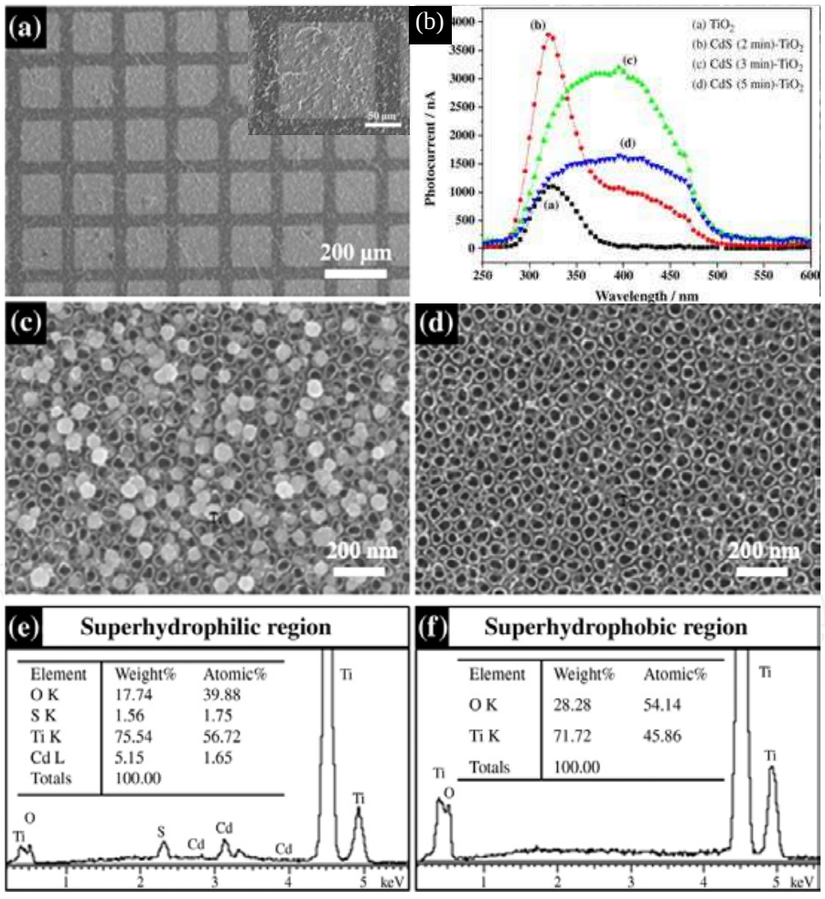

Fig. 16. (a) Typical SEM images of the CdS micropattern; (b) Photocurrent spectra of micropatterned CdS film on TiO_2 nanotube array electrode. (curve a-d): pure TiO_2; 2 min; 3 min; and 5 min. (c) Superhydrophilic region; (d) superhydrophobic region. EDX spectrum of the corresponding superhydrophilic (e) and superhydrophobic regions (f).

5. Summary and outlook

Extremely wetting micropattern (superhydrophilic/superhydrophobic) on TiO_2 nanostructure surface by using SAM technique and photocatalytic lithography has been studied intensely as it provides a cost effective template to construct well defined functional composited pattern. Numerous potential applications have also been proposed and investigated in biomedical, sensors and micro-nano devices. We believe that the photocatatlytic lithography patterning technique presented in this chapter should be general to create micro-scale wetting pattern on other semiconductor substrates and these developments will open the door for more widespread application of the wetting pattern in practical fields.

6. Acknowledgments

The authors thank the National Natural Science Foundation of China (grants 51072170, 21021002), the National Basic Research Program of China (grant 2007CB935603) and the National High Technology Research and Development Program of China (grant 2009AA03Z327), and the Environment and Water Industry Programme Office (EWI) under the National Research Foundation of Singapore (grant MEWR651/06/160) for their financial supports.

7. References

Balaur, E., Macak, J.M., Taveira, L. & Schmuki, P. (2005). Tailoring the wettability of TiO_2 nanotube layers. *Electrochem. Commun.,* Vol. 7, No. 10, 1066-1070, 1388-2481

Bearinger, J.P., Stone, G, Hiddessen, A.L., Dugan, L.C., Wu, L.G., Hailey, P., Conway, J.W., Kuenzler, T., Feller, L., Cerritelli, S. & Hubbell, J.A. (2009). Phototocatalytic lithography of poly(propylene sulfide) block copolymers: Toward high-throughput nanolithography for biomolecular arraying applications. *Langmuir,* Vol. 25, No. 2, 1238-1244, 0743-7463

Bhawalkar, S.P., Qian, J., Heiber, M.C. & Jia, L. (2010). Development of a colloidal lithography method for patterning nonplanar surfaces. *Langmuir,* Vol. 26, No. 22, 16662-16666, 0743-7463

Crawford, G.A. & Chawla, N. (2009). Porous hierarchical TiO_2 nanostructures: Processing and microstructure relationships. *Acta Mater.,* Vol. 57, No. 3, 854-867, 1359-6454

Csucs, G., Kunzler, T., Feldman, K., Robin, F. & Spencer, N.D. (2003). Microcontact printing of macromolecules with submicrometer resolution by means of polyolefin stamps. *Langmuir,* Vol. 19, No. 15, 6104-6109, 0743-7463

Cui, B. & Veres, T. (2007). Fabrication of metal nanoring array by nanoimprint lithography (NIL) and reactive ion etching. *Microelectron. Eng.,* Vol. 84, No. 5-8, 1544-1547, 0167-9317

Falconnet, D., Koenig, A., Assi, T. & Textor M. (2004). A combined photolithographic and molecular-assembly approach to produce functional micropatterns for applications in the biosciences. *Adv. Funct. Mater.,* Vol. 14, No. 8, 749-756, 1616-301X

Felidj, N., Aubard, J. & Levi, G. (1999). Discrete dipole approximation for ultraviolet-visible extinction spectra simulation of silver and gold colloids. *J. Chem. Phys.,* Vol. 111, No. 3, 1195-1208, 0021-9606

Gao, X.F. & Jiang, L. (2004). Water-repellent legs of water striders. *Nature,* Vol. 432, No. 7013, 36-36, 0028-0836

Gong, D.W., Grimes, C.A. & Varghese O.K. (2001). Titanium oxide nanotube arrays prepared by anodic oxidation. *J. Mater. Res.,* Vol. 16, No. 12, 3331-3334, 0884-2914

Haick, H. & Paz, Y. (2001). Remote photocatalytic activity as probed by measuring the degradation of self-assembled monolayers anchored near microdomains of titanium dioxide. *J. Phys. Chem. B*, Vol. 105, No. 15, 3045-3051, 1089-5647

Huang, L., Braunschweig, A.B., Shim, W., Qin, L.D., Lim, J.K., Hurst, S.J., Huo, F.W., Xue, C., Jong, J.W. & Mirkin, C.A. (2010). Matrix-assisted dip-pen nanolithography and polymer pen lithography. *Small,* Vol. 6, No. 10, 1077-1081, 1613-6810

Huang, Y.X., Lai, Y.K., Lin, L.X., Sun, L. & Lin, C.J. (2010). Electrochemical construction and biological performance of micropatterned CaP films. *Acta Phys. -Chim. Sin.,* Vol. 26, No. 8, 2057-2060, 1000-6818

Huang, Y.X., Sun, L., Xie, K.P., Lai, Y.K., Liu, B.J., Ren, B. & Lin, C.J. (2011). A SERS study of Ag nanoparticles electrodeposited on patterned TiO_2 nanotube films, *J. Raman Spectrosc.,* DOI: 10.1002/jrs.2830, 0377-0486, Vol. 42, No. 5, 986-991

Ichimura, K., Oh, S.K. & Nakagawa, M. (2000). Light-driven motion of liquids on a photoresponsive surface. *Science,* Vol. 288, No. 5471, 1624-1626, 0036-8075

Jeon, N.L., Clem, P.G., Payne, D.A. & Nuzzo, R.G. (1996). A monolayer-based lift-off process for patterning chemical vapor deposition copper thin films. *Langmuir*, Vol. 12, No. 22, 5350-5355, 0743-7463

Jiao, L.Y., Gao, H.J., Zhang, G.M., Xie, G.Y., Zhou, X., Zhang, Y.Y., Zhang, Y.Y., Gao, B., Luo, G., Wu, Z.Y., Zhu, T., Zhang, J., Liu, Z.F., Mu, S.C., Yang, H.F. & Gu, C.Z. (2005). Fabrication of metallic nanostructures by negative nanoimprint lithography. *Nanotechnology,* Vol. 16, No. 12, 2779-2784, 0957-4484

Katagiri, K., Ohno, K., Masuda, Y. & Koumoto, K. (2007). Growth behavior of TiO_2 particles via the liquid phase deposition process. *J. Ceram. Soc. Jpn.,* Vol. 115, No. 1348, 831-834, 1882-0743

Kobayashi, T., Shimizu, K., Kaizuma, Y. & Konishi, S. (2011). Formation of superhydrophobic/superhydrophilic patterns by combination of nanostructure-imprinted perfluoropolymer and nanostructured silicon oxide for biological droplet generation. *Appl. Phys. Lett.,* Vol. 98, No. 12, 123706, 0003-6951

Koumoto, K., Saito, N., Gao, Y.F., Masuda, Y. & Zhu, P.X. (2008). Nano/micro patterning of inorganic thin films. *Bull. Chem. Soc. Jpn.,* Vol. 81, No. 11, 1337-1376, 0009-2673

Kubo, W., Tatsuma, T., Fujishima, A. & Kobayashi, H. (2004). Mechanisms and resolution of photocatalytic lithography. *J. Phys. Chem. B*, Vol. 108, No. 9, 3005-3009, 1520-6106

Kumar, A., Biebuyck, H.A., Abbott, N.L. & Whitesides, G.M. (1992). The use of self-assembled monolayers and a selective etch to generate patterned gold features. *J. Am. Chem. Soc.,* Vol. 114, No. 23, 9188-9189, 0002-7863

Lafuma, A. & Quéré, D. (2003). Superhydrophobic states. *Nat. Mater.,* Vol. 2, No. 7, 457-460, 1476-1122

Li, L.Y., Yang, Y., Yang, G.L., Chen, X.M., Hsiao, B.S., Chu, B., Spanier, J.E. & Li, C.Y. (2006). Patterning polyethylene oligomers on carbon nanotubes using physical vapor deposition. *Nano Lett.,* Vol. 6, No. 5, 1007-1012, 1530-6984

Lai, Y.K., Sun, L., Zuo, J. & Lin, C.J. (2004). Electrochemical fabrication and formation mechanism of TiO_2 nanotube array on metallic titanium surface. *Acta Phys. -Chim. Sin.,* Vol. 20, No. 9, 1063-1066, 1000-6818

Lai, Y.K., Sun, L., Chen, Y.C., Zhuang, H.F., Lin, C.J. & Chin, J.W. (2006). Effects of the structure of TiO_2 nanotube array on Ti substrate on its photocatalytic activity. *J. Electrochem. Soc.,* Vol. 153, No. 7, D123-127, 0013-4651

Lai, Y.K., Lin, C.J., Wang, H., Huang, J.Y., Zhuang, H.F. & Sun, L. (2008). Superhydrophilic-superhydrophobic micropattern on TiO_2 nanotube films by photocatalytic lithography. *Electrochem. Commun.,* Vol. 10, No. 3, 387-391, 1388-2481

Lai, Y.K., Lin, C.J., Huang, J.Y., Zhuang, H.F., Sun, L. & Nguyen, T. (2008). Markedly controllable adhesion of superhydrophobic spongelike nanostructure TiO_2 films. *Langmuir,* Vol. 24, No. 8, 3867-3873, 0743-7463

Lai, Y.K., Gao, X.F., Zhuang, H.F., Huang, J.Y., Lin, C.J. & Jiang, L. (2009). Designing superhydrophobic porous nanostructures with tunable water adhesion. *Adv. Mater.,* Vol. 21, No. 37, 3799-3803, 0935-9648

Lai, Y.K., Huang, J.Y., Gong, J.J., Huang, Y.X., Wang, C.L., Chen, Z. & Lin, C.J. (2009). Superhydrophilic-superhydrophobic Template: A simple approach to micro- and nanostructure patterning of TiO_2 films. *J. Electrochem. Soc.,* Vol. 156, No. 11, D480-484, 0013-4651

Lai, Y.K., Zhuang, H.F., Sun, L., Chen, Z. & Lin, C.J. (2009). Self-organized TiO_2 nanotubes in mixed organic-inorganic electrolytes and their photoelectrochemical performance. *Electrochim. Acta,* Vol. 54, No. 26, 6536-6542, 0013-4686

Lai, Y.K., Lin, Z.Q., Huang, J.Y., Sun, L., Chen, Z. & Lin, C.J. (2010). Controllable construction of ZnO/TiO_2 patterning nanostructures by superhydrophilic/superhydrophobic templates. *New J. Chem.,* Vol. 34, No. 1, 44-51, 1144-0546

Lai, Y.K., Huang, J.Y., Zhang, H.F., Subramaniam, V.P., Tang, Y.X., Gong, D.G., Sundar, L., Sun, L., Chen, Z. & Lin, C.J. (2010). Nitrogen-doped TiO_2 nanotube array films with enhanced photocatalytic activity under various light sources. *J. Hazard. Mater.,* Vol. 184, No. 1-3, 855-863, 0304-3894

Lai, Y.K., Huang, Y.X., Huang, J.Y., Wang, H., Chen, Z. & Lin, C.J. (2010). Selective formation of ordered arrays of octacalcium phosphate ribbons on TiO_2 nanotube surface by template-assisted electrodeposition. *Colliods Surf. B,* Vol. 76, No. 1, 117-122, 0927-7765

Lai, Y.K., Lin, Z.Q., Chen, Z., Huang, J.Y. & Lin, C.J. (2010). Fabrication of patterned CdS/TiO_2 heterojunction by wettability template-assisted electrodeposition. *Mater. Lett.,* Vol. 64, No. 11, 1309-1312, 0167-577X

Lee, J.P. & Sung, M.M. (2004). A new patterning method using photocatalytic lithography and selective atomic layer deposition. *J. Am. Chem. Soc.,* Vol. 126, No. 1, 28-29, 0002-7863

Lee, S.W., Oh, B.K., Sanedrin, R.G., Salaita, K., Fujigaya, T. & Mirkin, C.A. (2006). Biologically active protein nanoarrays generated using parallel dip-pen nanolithography. *Adv. Mater.,* Vol. 18, No. 9, 1133-1136, 0935-9648

Li, Z.W., Gu, Y.N., Wang, L., Ge, H.X., Wu, W., Xia, Q.F., Yuan, C.S., Chen, Y., Cui, B. & Williams, R.S. (2009). Hybrid nanoimprint-soft lithography with sub-15 nm resolution. *Nano Lett.,* Vol. 9, No. 6, 2306-2310, 1530-6984

Liu, S.H., Wang, W.C.M., Mannsfeld, S.C.B., Locklin, J., Erk, P., Gomez, M., Richter, F. & Bao, Z.N. (2007). Solution-assisted assembly of organic semiconducting single crystals on surfaces with patterned wettability. *Langmuir,* Vol. 23, No. 14, 7428-7432, 0743-7463

Liu, M.J., Zheng, Y.M., Zhai, J. & Jiang, L. (2010). Bioinspired super-antiwetting interfaces with special liquid-solid adhesion. *Accounts Chem. Res.,* Vol. 43, No. 3, 368-377, 0001-4842

Liu, X.J., Ye, Q.A., Yu, B., Liang, Y.M., Liu, W.M. & Zhou, F. (2010). Switching water droplet adhesion using responsive polymer brushes. *Langmuir,* Vol. 26, No. 14, 12377-12382, 0743-7463

Lu, Y., Liu, G.L. & Lee, L.P. (2005). High-density silver nanoparticle film with temperature-controllable interparticle spacing for a tunable surface enhanced Raman scattering substrate. *Nano Lett.,* Vol. 5, No. 1, 5-9, 1530-6984

Masuda, Y., Kinoshita, N., Sato, F. & Koumoto, K. (2006). Site-selective deposition and morphology control of UV- and visible-light-emitting ZnO crystals. *Cryst. Growth Des.,* Vol. 6, No. 1, 75-78, 1528-7483

Michel, R., Reviakine, I., Sutherland, D., Fokas, C., Csucs, G., Danuser, G., Spencer, N.D. & Textor, M. (2002). A novel approach to produce biologically relevant chemical patterns at the nanometer scale: Selective molecular assembly patterning combined with colloidal lithography. *Langmuir,* Vol. 18, No. 22, 8580-8586, 0743-7463

Nakata, K., Nishimoto, S., Yuda, Y., Ochiai, T., Murakami, T. & Fujishima, A. (2010). Rewritable superhydrophilic-superhydrophobic patterns on a sintered titanium dioxide substrate. *Langmuir,* Vol. 26, No. 14, 11628-11630, 0743-7463

Nishimoto, S., Sekine, H., Zhang, X.T., Liu, Z.Y., Nakata, K., Murakami, T., Koide, Y. & Fujishima, A. (2009). Assembly of self-assembled monolayer-coated Al_2O_3 on TiO_2 thin films for the fabrication of renewable superhydrophobic-superhydrophilic structures. *Langmuir,* Vol. 25, No. 13, 7226-7228, 0743-7463

Rausch, N. & Burte, E.P. (1993). Thin TiO_2 films prepared by low-pressure chemical vapor-deposition. *J. Electrochem. Soc.,* Vol. 140, No. 1, 145-149, 0013-4651

Rusponi, S., Costantini, G., de Mongeot, F.B., Boragno, C. & Valbusa, U. (1999). Patterning a surface on the nanometric scale by ion sputtering. *Appl. Phys. Lett.,* Vol. 75, No. 21, 3318-3320, 0003-6951

Shen, G.X., Chen, Y.C. & Lin, C.J. (2005). Corrosion protection of 316 L stainless steel by a TiO_2 nanoparticle coating prepared by sol-gel method. *Thin Solid Films,* Vol. 489, No. 1-2, 130-136, 0040-6090

Slocik, J.M., Beckel, E.R., Jiang, H., Enlow, J.O., Zabinski, J.S., Bunning, T.J. & Naik, R.R. (2006). Site-speciric patterning of biomolecules and quantum dots on functionalized surfaces generated by plasma-enhanced chemical vapor deposition. *Adv. Mater.,* Vol. 18, No. 16, 2095-2100, 0935-9648

Takeda, S., Suzuki, S., Odaka, H. & Hosono, H. (2001). Photocatalytic TiO_2 thin film deposited onto glass by DC magnetron sputtering. *Thin Solid Films,* Vol. 392, No. 2, 338-344, 0040-6090

Tatsuma, T., Kubo, W. & Fujishima, A. (2002). Patterning of solid surfaces by photocatalytic lithography based on the remote oxidation effect of TiO_2. *Langmuir,* Vol. 18, No. 25, 9632-9634, 0743-7463

Wang, H., Lin, C.J., Hu, R., Zhang, F. & Lin, L.W. (2008). A novel nano-micro structured octacalcium phosphate/protein composite coating on titanium by using an electrochemically induced deposition. *J. Biomed. Mater. Res. A,* Vol. 87A, No. 3, 698-705, 1549-3296

Wang, H., Duan, J.C. & Cheng, Q. (2011). Photocatalytically patterned TiO_2 arrays for on-plate selective enrichment of phosphopeptides and direct MALDI MS analysis. *Anal. Chem.,* Vol. 83, No. 5, 1624-1631, 0003-2700

Wang, R., Hashimoto, K., Fujishima, A., Chikuni, M., Kojima, E., Kitamura, A., Shimohigoshi, M. & Watanabe, T. (1997). Light-induced amphiphilic surfaces. *Nature,* Vol. 388, No. 6641, 431-432, 0028-0836

Wang, Y.L. & Lieberman, M. (2003). Growth of ultrasmooth octadecyltrichlorosilane self-assembled monolayers on SiO_2. *Langmuir,* Vol. 19, No. 4, 1159-1167, 0743-7463

West, J.B. (1999). The original presentation of Boyle's law. *J. Appl. Physiol.,* Vol. 87, No. 4, 1543-1545, 8750-7587

Xu, S. & Liu, G.Y. (1997). Nanometer-scale fabrication by simultaneous nanoshaving and molecular self-assembly. *Langmuir,* Vol. 13, No. 2, 127-129, 0743-7463

Yang, Y., Lai, Y.K., Zhang, Q.Q., Wu, K., Zhang, L.H., Lin, C.J. & Tang, P.F. (2010). A novel electrochemical strategy for improving blood compatibility of titanium-based biomaterials. *Colloids Surf. B,* Vol. 79, No. 1, 309-313, 0927-7765

Yasuda, K., Macak, J.M., Berger, S., Ghicov, A. & Schmuki, P. (2007). Mechanistic aspects of the self-organization process for oxide nanotube formation on valve metals. *J. Electrochem. Soc.,* Vol. 154, No. 9, C472-478, 0013-4651

Yoshimura, M. & Gallage, R. (2008). Direct patterning of nanostructured ceramics from solution - differences from conventional printing and lithographic methods. *J. Solid State Electrochem.,* Vol. 12, No. 7-8, 775-782, 1432-8488

Yun, H., Lin, C.J., Li, J. Wang, J.R. & Chen, H.B. Low-temperature hydrothermal formation of a net-like structured TiO_2 film and its performance of photogenerated cathode protection. *Appl. Surf. Sci.,* Vol. 255, No. 5, 2113-2117, 0169-4332

Zeng, J.B., Jia, H.Y., An, J., Han, X.X., Xu, W.Q., Zhao, B. & Ozaki, Y. (2008). Preparation and SERS study of triangular silver nanoparticle self-assembled films. *J. Raman Spectrosc.,* Vol. *39*, No. 11, 1673-1678, 0377-0486

Zhang, C. & Kalyanaraman, R. (2004). In situ lateral patterning of thin films of various materials deposited by physical vapor deposition. *J. Mater. Res.,* Vol. 19, No. 2, 595-599, 0884-2914

Zhang, G.M., Zhang, J., Xie, G.Y., Liu, Z.F. & Shao H.B. (2006). Cicada wings: A stamp from nature for nanoimprint lithography. *Small,* Vol. 2, No. 12, 1440-1443, 1613-6810

Zhang, G.J., Tanii, T., Kanari, Y. & Ohdomari, I. (2007). Production of nanopatterns by a combination of electron beam lithography and a self-assembled monolayer for an antibody nanoarray. *J. Nanosci. Nanotechnol.,* Vol. 7, No. 2, 410-417, 1533-4880

Zhang, X.T., Jin, M., Liu, Z.Y., Tryk, D., Nishimoto, S., Murakami, T. & Fujishima, A. (2007). Superhydrophobic TiO_2 surfaces: Preparation, photocatalytic wettability conversion, and superhydrophobic-superhydrophilic patterning. *J. Phys. Chem. C,* Vol. 111, No. 39, 14521-14529, 1932-7447

Zhao, J.C., Wu, T.X., Wu, K.Q., Oikawa, K., Hidaka, H. & Serpone, N. (1998). Photoassisted degradation of dye pollutants. 3. Degradation of the cationic dye rhodamine B in aqueous anionic surfactant/TiO_2 dispersions under visible light irradiation: Evidence for the need of substrate adsorption on TiO_2 particles. *Environ. Sci. Technol.,* Vol. 32, No. 16, 2394-2400, 0013-936X

Zhuang, H.F., Lin, C.J., Lai, Y.K., Sun, L. & Li, J. (2007). Some critical structure factors of titanium oxide manotube array in its photocatalytic activity. *Environ. Sci. Technol.,* Vol. 41, No. 13, 4735-4740, 0013-936X

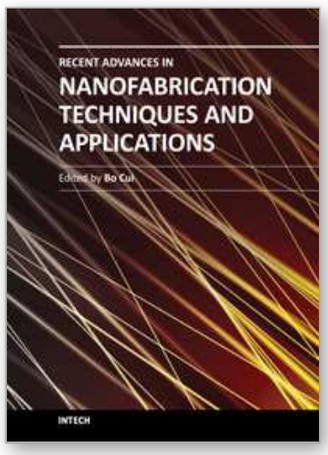

Recent Advances in Nanofabrication Techniques and Applications
Edited by Prof. Bo Cui

ISBN 978-953-307-602-7
Hard cover, 614 pages
Publisher InTech
Published online 02, December, 2011
Published in print edition December, 2011

Nanotechnology has experienced a rapid growth in the past decade, largely owing to the rapid advances in nanofabrication techniques employed to fabricate nano-devices. Nanofabrication can be divided into two categories: "bottom up" approach using chemical synthesis or self assembly, and "top down" approach using nanolithography, thin film deposition and etching techniques. Both topics are covered, though with a focus on the second category. This book contains twenty nine chapters and aims to provide the fundamentals and recent advances of nanofabrication techniques, as well as its device applications. Most chapters focus on in-depth studies of a particular research field, and are thus targeted for researchers, though some chapters focus on the basics of lithographic techniques accessible for upper year undergraduate students. Divided into five parts, this book covers electron beam, focused ion beam, nanoimprint, deep and extreme UV, X-ray, scanning probe, interference, two-photon, and nanosphere lithography.

How to reference
In order to correctly reference this scholarly work, feel free to copy and paste the following:

Yuekun Lai, Changjian Lin and Zhong Chen (2011). Extremely Wetting Pattern by Photocatalytic Lithography and Its Application, Recent Advances in Nanofabrication Techniques and Applications, Prof. Bo Cui (Ed.), ISBN: 978-953-307-602-7, InTech, Available from: http://www.intechopen.com/books/recent-advances-in-nanofabrication-techniques-and-applications/extremely-wetting-pattern-by-photocatalytic-lithography-and-its-application

INTECH
open science | open minds

InTech Europe
University Campus STeP Ri
Slavka Krautzeka 83/A
51000 Rijeka, Croatia
Phone: +385 (51) 770 447
Fax: +385 (51) 686 166
www.intechopen.com

InTech China
Unit 405, Office Block, Hotel Equatorial Shanghai
No.65, Yan An Road (West), Shanghai, 200040, China
中国上海市延安西路65号上海国际贵都大饭店办公楼405单元
Phone: +86-21-62489820
Fax: +86-21-62489821

IntechOpen